

# Neutrino Dimuon Data and the Strangeness Content of the Nucleon

F. Olness<sup>a</sup>, J. Pumplin<sup>b</sup>, D. Stump<sup>b</sup>, J. Huston<sup>b</sup>, P. Nadolsky<sup>a</sup>, H. L. Lai<sup>c</sup>,  
S. Kretzer<sup>d</sup>, J. F. Owens<sup>e</sup>, W. K. Tung<sup>b</sup>

<sup>a</sup>Department of Physics, Southern Methodist University

<sup>b</sup>Department of Physics and Astronomy, Michigan State University

<sup>c</sup>Taipei Municipal Teachers College, Taiwan

<sup>d</sup>Physics Department and RIKEN-BNL Research Center, Brookhaven National Laboratory

<sup>e</sup>Department of Physics, Florida State University

We have performed the first comprehensive global QCD analysis including the CCFR and NuTeV dimuon data, which provide direct constraints on the strange and anti-strange parton distributions  $s(x)$ ,  $\bar{s}(x)$ . To fully explore the strangeness sector, we adopt a very general parametrization of the non-perturbative  $s(x)$ ,  $\bar{s}(x)$  functions satisfying basic QCD requirements. This global analysis yields several classes of solutions that are consistent with current theoretical and experimental constraints. A robust feature of the acceptable fits is that the strangeness asymmetry, as measured by the momentum integral  $[S^-] \equiv \int_0^1 x[s(x) - \bar{s}(x)]dx$ , is in the positive range 0.0010 to 0.0030. The limits of  $[S^-]$  consistent with current experimental and theoretical constraints are further studied by using the Lagrange Multiplier method, which is designed to cover the entire strangeness parameter space. These results have a direct impact on the QCD corrections to the Paschos-Wolfenstein relation, which is used in the measurement of the Weinberg angle  $\sin \theta_W$  in  $\nu N$  and  $\bar{\nu} N$  scattering.

## Introduction

The recent measurements of both neutrino and anti-neutrino production of dimuons (mainly due to charm final states) by the CCFR and NuTeV collaborations [1] provide the first direct experimental constraints on the strange and anti-strange quark distributions  $s(x)$  and  $\bar{s}(x)$  of the nucleon. In addition to the intrinsic interest in nucleon structure, the strange asymmetry ( $s - \bar{s}$ ) has important implications on the precision measurement of the Weinberg angle.[2] We report here the first comprehensive global QCD analysis that includes the CCFR and NuTeV dimuon data, using the powerful Hessian and Lagrange methods to explore the entire strange and anti-strange parton parameter space.

In previous global analyses, information on  $s$  and  $\bar{s}$  resides only in inclusive cross sections for neutral and charged current DIS. The reliability of the extraction of the quite small  $s$  and  $\bar{s}$  contributions was always in considerable doubt. For this reason, most global fits adopt the assumption  $s(x) = \bar{s}(x) \sim \kappa(\bar{u} + \bar{d})/2$  (with  $\kappa \sim 0.5$ ) at some low value of  $Q$ , which was inferred from the earlier combined neutrino and antineutrino dimuon experiments. The recent high-statistics dimuon measurements of [1] provide greater accuracy, as well as the first opportunity to study the difference  $s(x) - \bar{s}(x)$ . Neutrino induced dimuon production,  $\nu/\bar{\nu}N \rightarrow \mu^+\mu^-X$ , proceeds primarily through the subprocess  $W^+s \rightarrow c$  and  $W^-\bar{s} \rightarrow \bar{c}$  respectively, and hence provides independent information on  $(s, \bar{s})$ .

We present a global analysis including this new dimuon data, corrected for experimental cuts and efficiencies using information provided by the experimental group [1]. The new results prove to be rich in physical content, due to the interplay of the enhanced experimental constraints and the strong theoretical requirements of PQCD.

We begin by describing the general features of the strangeness sector of the nucleon structure in the QCD framework, and our general parametrization of that sector. This will be followed by the main results of the global analysis, with emphasis on the strangeness asymmetry. The paper concludes with comparison to previous work and a summary.

## General properties of $(s - \bar{s})(x)$ and its first two moments

For each  $Q$ , let us define the strangeness number densities  $s^\pm(x)$  and their integrals  $[s^\pm]$  by

$$[s^\pm] \equiv \int_0^1 s^\pm(x) dx \equiv \int_0^1 [s(x) \pm \bar{s}(x)] dx , \quad (1)$$

and the momentum densities  $S^\pm(x)$  and integrals  $[S^\pm]$  by

$$[S^\pm] \equiv \int_0^1 S^\pm(x) dx \equiv \int_0^1 x[s(x) \pm \bar{s}(x)] dx . \quad (2)$$

In the QCD parton model, we expect,

1. The parton distributions  $s$  and  $\bar{s}$  (or equivalently  $s^\pm$ ), are parametrized at *one particular* initial  $Q_0$ ; the full  $Q$ -dependence is then determined by QCD evolution.

2. The strangeness number sum rule for the nucleon requires  $[s^-] = 0$  (for all  $Q$ ). A necessary condition is that  $s^-(x)$  be less singular than  $1/x$  as  $x \rightarrow 0$  for all  $Q$ .
3. The momentum sum rule requires:  $[S^+] + \Sigma_0 = 1$  where  $\Sigma_0$  represents the momentum fraction of all non-strange partons; this condition strongly constrains  $[S^+]$  because  $\Sigma_0$  is rather well determined by DIS and other experiments.
4. In the limit  $x \rightarrow 0$  (high energy and fixed  $Q$ ), Regge considerations suggest  $s^-(x)/s^+(x) \rightarrow 0$ .

From these general constraints, we draw the following conclusions:

- The number sum rule, (1), implies that the curve of  $s^-(x)$  must cross the  $x$ -axis *at least once* in the interval  $[0, 1]$ ; and the areas bounded by the curve above and below the  $x$ -axis must be equal;
- Assuming only one crossing at  $x = x_0$ , then  $s^-(x) < 0$  for small  $x$  implies  $[S^-] > 0$ ; and vice versa. This is, of course, a simple consequence of the fact that the momentum integral suppresses the small  $x$  region and enhances the large  $x$  region. Fig. (1), taken from typical solutions to be discussed later, makes this point explicit.
- Because the experimental constraints are weak in the small  $x$  region, the detailed behavior of  $s^-(x)$  is unconstrained in this region, as shown by the various classes of solutions displayed in the upper plot of Fig. 1. However, this uncertainty is of little consequence for  $S^-(x)$ , as explicitly demonstrated by the curves of the lower plot. Thus the general conclusion concerning the sign of  $[S^-]$  is expected to be robust.

The CCFR-NuTeV dimuon study [1, 3] suggested that  $s^-(x) < 0$  in the bulk of the  $x$  range covered by the experiment ( $0.01 < x < 0.3$ ). A previous detailed global analysis of inclusive data by Barone et al. [4] (henceforth referred to as BPZ), finds that  $s^-(x) > 0$  in the larger  $x$  region. These results, combined with the theoretical constraints discussed above, lead naturally to the conclusion  $[S^-] > 0$ . The magnitude of  $[S^-]$  will depend on the crossing point and the precise shape of the  $s^-(x)$  curve.

## General parametrization of the strangeness distributions

To explore the strangeness sector of the parton structure of the nucleon, we need a suitable parametrization of  $s$  and  $\bar{s}$  (or equivalently  $s^\pm$ ) at the fixed scale  $Q_0$ . This parametrization must satisfy the theoretical requirements specified above, and it should be as general as possible so that the allowed space can be fully covered. A general functional form is essential, so that our conclusions are not simply artifacts of the parametrization, but truly characterize the underlying experimental data and the PQCD theory.

It is more natural to parametrize the  $s^\pm(x, Q_0)$  functions independently (rather than  $s$  and  $\bar{s}$ ) since they satisfy different QCD evolution equations—pure non-singlet (for  $s^-$ ) and mixed singlet/non-singlet (for  $s^+$ ). We use the following parametrization,

$$s^+(x, Q_0) = A_0 x^{A_1} (1-x)^{A_2} P_+(x; A_3, A_4, \dots) \quad (3)$$

$$s^-(x, Q_0) = s^+ \tanh[a x^b (1-x)^c P_-(x; x_0, d, e, \dots)] \quad (4)$$

where  $P_+(x; A_3, \dots)$  is a positive definite, smooth function in the interval  $(0, 1)$ , depending on additional parameters  $A_3, \dots$  (such as that used for  $u, d, g, \dots$  in most CTEQ [5] and other global analyses [6, 7]), and

$$P_-(x) = \left(1 - \frac{x}{x_0} + dx^2 + ex^3 + \dots\right) \quad (5)$$

where the parameter  $x_0$  is to be determined by the strangeness number sum rule  $[s^-] = 0$ , and the parameters  $d, e, \dots$  are optional, depending on how much detail is accessible with the existing constraints. Important features of this parametrization are the following.

- The strangeness quantum number sum rule,  $[s^-] = 0$ , is satisfied by the choice of  $x_0$ . The parameter  $x_0$  has a physical interpretation in the simple three-parameter case (i.e.  $a, b, c$ , only): it is precisely the “crossing point” where  $s^-(x) = 0$  mentioned before.
- The fact that the tanh function has absolute value less than 1 ensures positivity of  $s(x)$  and  $\bar{s}(x)$ . The fact that tanh is a monotonic function guarantees that the function  $s^-(x)$  can be made as general as necessary by the choice of  $P_-(x)$ .
- The small- $x$  behavior of  $s^-(x)$  must be such that the integral  $[s^-]$  converges (before the root  $x_0$  is determined). This is guaranteed if the parameter  $b$  is chosen in the range  $A_1 + b > -1$ , because Eq.(4) implies that  $s^-(x) \sim x^{A_1+b}$  as  $x \rightarrow 0$ .

Because  $P_\pm(x)$  can be made as general as necessary, the choice in Eqs.(3–5) is capable of exploring the full strangeness parameter space allowed by data in the PQCD framework.

## Global Analysis

We now describe the global QCD analysis, which includes all relevant experimental data and implements the theoretical ideas outlined above. This may be considered an extension of the on-going CTEQ program of global analysis. Several new elements (compared to the latest CTEQ6M[5] and CTEQ6HQ[8] analyses) are present. On the experimental side, we have added the CDHSW inclusive  $F_2$  and  $F_3$  data sets [9], the CCFR-NuTeV dimuon data sets [1] and the new E866  $pp$  Drell-Yan data set [10]. On the theoretical side, we have expanded the parameter space to include the strangeness sector as discussed above.

Compared to the global analyses of BPZ [4] that have allowed  $s \neq \bar{s}$ , the major difference experimentally is our inclusion of the dimuon data that give direct handles on  $s$  and  $\bar{s}$ , and, theoretically, the generality and naturalness of our parametrization of the strange distributions.<sup>a</sup>

The inclusion of the CCFR-NuTeV neutrino and anti-neutrino dimuon production data in a global QCD analysis is not a straightforward task: the experimental measurement is presented as a series of “forward differential cross sections” with experimental cuts, whereas the theoretical quantities that are most directly related to the parton distribution analysis are the underlying “charm quark production cross sections”. The gap between the two is

---

<sup>a</sup>Ref.[4] parametrizes, in simple forms,  $s(x)$  and  $\bar{s}(x)$  separately, rather than  $s^\pm(x)$ . Cf. discussion of last section.

usually bridged by Monte Carlo programs that incorporate experimental cuts and efficiencies as well as fragmentation models. In our analysis, we rely on a Pythia program provided by the CCFR-NuTeV collaboration.<sup>b</sup> This Monte Carlo calculation is done in the spirit and the framework of leading-order (LO) QCD. Accordingly, the theoretical formulas used are also in LO. Since, as will be shown in the results sections, the uncertainties of existing experimental constraints are quite large, the LO treatment is quite adequate for this study of the dimuon data within a global QCD analysis. Needless to say, all fully inclusive (large) cross sections used in this study are treated in NLO QCD, as in all modern global analyses.

**Procedure** Our analysis is carried out in several stages.

1. We first fix all of the “conventional” parton parameters to their values in the CTEQ6M parton distribution set, and fit the complete set of data by varying only the parameters associated with the new degrees of freedom in  $s^-$ . We observe that: (i) most of the data sets used in the previous analysis are not affected at all by the variation in  $s^-$  (as they should not be); (ii) a few fully inclusive cross sections are slightly affected by the variation of  $s^-$  (such as  $F_3$  which depends on  $u - \bar{u} + d - \bar{d} + s - \bar{s} \dots$ ), but the sensitivities are weak; and (iii) the CCFR-NuTeV dimuon data sets are the most constraining ones for fitting  $s^-$ . We obtain good fits using the 3-parameter ( $a, b, c$ ) or the 4- or 5-parameter ( $a, b, c, d, e$ ) versions of Eqs.(4,5). There is not enough constraint to choose among these. The higher-order polynomials allow oscillatory behavior of  $s^-(x)$  which the 3-parameter form does not.
2. Using these candidate fits as a basis, we perform a second round of fitting allowing the parameters associated with  $s^+$ , Eq.(3), to vary in addition to the previous ones. This improves the fit to all data sets slightly. We observe that the shape of  $s^+(x)$  now deviates from the starting configuration where  $s^+(x)$  was set proportional to  $\bar{u}(x) + \bar{d}(x)$ . Defining the “kappa” parameter  $\kappa$  as the ratio of the momentum fraction carried by the strange quarks,  $[S^+]$ , to that carried by  $\bar{u} + \bar{d}$  at  $Q_0$  (chosen as  $Q_0 = 1.3$  GeV in our study), we find that  $\kappa$  may vary in the range 0.3–0.5;  $\chi^2$  has a shallow minimum around  $\kappa = 0.4$ . This result agrees with other analyses.

Because the experimental constraints are not sufficient to uniquely determine all the  $s^-$  and  $s^+$  parameters, we categorize several classes of equally good solutions based on factors such as whether  $s^-(x)$  has one or two crossing points, and the behavior of  $s^-(x)/s^+(x)$  as  $x \rightarrow 0$  or  $x \rightarrow 1$ .

3. We finalize these classes of solutions by allowing all parton parameters to vary so the non-strange parton distributions can adjust themselves to yield the best fit to all the experimental data sets. (As one would expect, the adjustments are generally small.) The differences in the  $\chi^2$  values between the various categories of solutions are not significant.

---

<sup>b</sup>We thank Tim Bolton and Max Goncharov, in particular, for providing this program, as well as assistance in its use. Their help was vital for carrying out this project.

**Results** The following description of results is based on a few representative examples chosen from a large number of candidate fits obtained by the above procedure. Since the quality of the fits to the global data sets other than the CCFR-NuTeV dimuon data remains quite similar to the previous CTEQ6M analysis, we focus our discussion on the strangeness sector. Specifically, we examine closely the asymmetry functions  $s^-(x)$ ,  $S^-(x)$  and the momentum integral  $[S^-]$ . The asymmetry functions from three typical good fits, with different small  $x$  behaviors (labelled as class A,B,C), have been shown in Fig. (1) as illustrations in the previous section.

In the accompanying table, for each sample fit, we list the small- $x$  exponent ( $A_1 + b$ ), the integrated momentum fraction ( $[S^-]$ ), and the relative  $\chi^2$  values normalized to that of solution B, which we use as the reference for comparison purposes. (Under column “B”, we give the absolute  $\chi^2$ ’s in parentheses.) To gain some insight on the constraints on the strangeness sector due to the various types of experiments, we show separately the  $\chi^2$  values for the dimuon data sets, the inclusive data sets (I) that are expected to be somewhat sensitive to  $s^-$  (consisting of the CCFR and CDHSW  $F_3(x, Q)$  and the CDF  $W$ -lepton asymmetry measurements), and the remaining ones (II) that are only indirectly affected by  $S^-$  (the rest of the inclusive data sets).

	# pts	B+	A	B	C	B-
$A_1 + b$	-	-0.78	-0.99	-0.78	0	-0.78
$[S^-] \times 100$	-	0.540	0.312	0.160	0.103	-0.177
Dimuon	174	<b>1.30</b>	1.02	1.00 (126)	1.01	<b>1.26</b>
Inclusive I	194	0.98	0.97	1.00 (141)	1.03	<b>1.09</b>
Inclusive II	2097	1.00	1.00	1.00 (2349)	1.00	1.00

Table 1. Features of the representative parton distribution sets described in the text. Arranged by the order of the value of  $[S^-]$  from left to right.

Focusing on the three good fits {A, B, C} first, we note the following.

- All three solutions {A, B, C} feature positive  $[S^-]$ ; and the more singular  $s^-(x)$  is as  $x \rightarrow 0$ , the higher the value of  $[S^-]$ . These are natural consequences of the strangeness sum rule (equal +/- areas under the curve of  $s^-(x)$ ) and the small  $x$  suppression of the momentum integral.
- Solution B is slightly favored over the other two. This, plus the fact that its small- $x$  behavior lies in the middle of the favored range, are the reasons for using it as the reference fit.
- We chose these examples among fits with the simplest parametrizations; all cross the  $x$  axis only once. With 4- or 5-parameters, many solutions can be found that entail oscillatory  $s^-(x)$ . But since the  $\chi^2$  values do not improve in a statistically significant way, we deem it premature to dwell on complicated behaviors, which may be mere artifacts of the parametrization rather than physical constraints.

**Can  $[S^-]$  be negative? And how large can  $[S^-]$  get?** These are important questions for their implications in precision measurement of the Weinberg angle in neutrino scattering.[2, 4, 11, 12, 13] We can study this problem in a quantitative way by applying the powerful Lagrange Multiplier (LM) method [14] in our global analysis. The B+ and B- solutions listed in Table 1 are obtained in the LM method by exploring the entire strangeness parameter space. The B- solution was obtained by forcing  $[S^-] = -0.0018$  (to be compared to  $-0.0027$  cited by [2, 12]). The B+ solution was generated by forcing  $[S^-]$  to go in the other direction until the increment of the overall  $\chi^2$  become comparable to that of B-; this results in  $[S^-] = 0.0054$ .

We see from the relevant entries in Table 1 that: (i) the  $\chi^2$  values of the dimuon data sets increase by about 30% in both cases; (ii) the “inclusive I” data sets disfavor the negative  $[S^-]$ ; and (iii) the “inclusive II” data sets are completely neutral. The two LM examples are chosen from a large number of fits spanning the entire strangeness parameter space. The pattern of dependence of the  $\chi^2$  values on the value of  $[S^-]$  is nearly universal. This observation is made explicit in Fig.(2), where the square points represent the (relative)  $\chi^2$  values of the dimuon data sets, and the triangle points of the “inclusive I” data sets. Not shown are those for the “inclusive II” data sets, which remain flat (at 1.00).

We see from this figure that the dimuon data sets favor a range of  $[S^-]$  centered around 0.0017, whereas the “inclusive I” data sets disfavor negative and low values of  $[S^-]$ . Taken together, a reasonable allowed range for  $[S^-]$  appears to be 0.001–0.003, although a value of zero (no strangeness asymmetry) is not necessarily ruled out. Sizable negative values of  $[S^-]$  are clearly disfavored. Cf. also Table 1.

The parton distribution functions associated with the sample sets listed in Table 1 will be made available on the CTEQ web page (<http://cteq.org>).

## Comparisons to previous studies

A comprehensive global QCD analysis with emphasis on the strangeness sector has been carried out previously by BPZ [4].<sup>c</sup> Without the dimuon data, which are directly sensitive to strangeness, the results of BPZ implicitly rely on small differences between large neutral- and charged-current inclusive cross sections from different experiments. The latest representative  $s^-(x)$  and  $S^-(x)$  functions extracted by BPZ (the solution “with CCFR (inclusive data)”) are shown in Fig.(3), along with our reference fit B. The main feature of the BPZ curves is a positive bump at rather large  $x$ . This has been attributed to the influence of the CDHSW data (which we also include in our analysis). Their conclusion that data favor a positive value of the momentum integral  $[S^-]$  is in agreement with our detailed study based on the LM method. The difference in the position of the positive peak can be attributed to: (i) the CCFR-NuTeV dimuon data (which were not included in the BPZ analysis); and (ii) the

---

<sup>c</sup>BPZ works directly with DIS cross sections (instead of structure functions), with detailed attention to systematic errors and other sources of uncertainties.

relative flexibility of the respective parametrization of the non-perturbative input functions (cf. discussion in earlier sections).

The CCFR-NuTeV experiments performed separate and combined analysis of  $s$  and  $\bar{s}$ , [1], based on their own dimuon and inclusive cross sections. To parameterize the  $s(x)$  and  $\bar{s}(x)$  distributions, they chose

$$\begin{pmatrix} s(x, Q) \\ \bar{s}(x, Q) \end{pmatrix} = \frac{\bar{u}(x, Q) + \bar{d}(x, Q)}{2} \begin{pmatrix} \kappa(1-x)^\alpha \\ \bar{\kappa}(1-x)^{\bar{\alpha}} \end{pmatrix}$$

for all  $\{x, Q\}$ .

Curves representing the general behavior of this model, with parameters  $(\kappa, \bar{\kappa}, \alpha, \bar{\alpha})$  taken from [1], at  $Q^2 = 10 \text{ GeV}^2$ , are given in Fig.(3) for comparison with the other results. While this model might be acceptable for a limited range of  $x$  and  $Q$ , it leads to serious problems in general: (i) the strangeness number sum rule  $[s^-] = 0$  is badly violated (the integral  $[s^-]$  diverges unless  $\kappa = \bar{\kappa}$ ), as is the momentum sum rule; (ii) the QCD evolution equation is violated at LO.<sup>d</sup> Problem (i) can be clearly seen in Fig.(3).

For these reasons, the “ $s(x, Q)$ ” and “ $\bar{s}(x, Q)$ ” functions extracted from this analysis cannot be directly related to the QCD strange and anti-strange parton distributions over a wide range of  $\{x, Q\}$ . Properly extending the strange distributions in  $x$  beyond the range of the dimuon data to satisfy the parton number and momentum sum rules, as well as defining the parametrization at a fixed  $Q = Q_0$  and letting QCD determine the  $Q$  dependence, are essential for making inferences on the physical strange and anti-strange quarks in general.

## Conclusion

We find several classes of solutions in the strangeness sector that are consistent with all relevant world data used in the global analysis. The dimuon data are vital in constraining the strangeness asymmetry parameters. The constraints provided by other inclusive measurements, labelled as “inclusive I” in the text, are consistent with those provided by dimuon data; and they are mutually complementary. (Cf. Fig.(2).) The allowed solutions generally prefer the momentum integral  $[S^-] \equiv \int_0^1 x[s(x) - \bar{s}(x)] dx$  to be positive. This conclusion is quite robust, and it follows from the basic properties of PQCD and from qualitative features of the experimental data. The size of this strangeness asymmetry is  $1-3 \times 10^{-3}$ . Furthermore, the Lagrange Multiplier method explicitly demonstrates that both the dimuon data and the other global analysis data sets strongly disfavor a negative  $[S^-]$ .

This result has significant implications for the extraction of the weak mixing angle,  $\sin \theta_W$ ; these details will be presented separately in Ref. [15].

---

<sup>d</sup>Contrary to the discussions in [2], these problems have nothing to do with a LO vs. NLO analysis.

## Acknowledgment

We thank members of CCFR and NuTeV collaboration, in particular T. Bolton and M. Goncharov, for discussions about the dimuon data, and assistance in their use. We also thank Benjamin Porthault for discussions of the BPZ work and for assistance in generating their results for comparison. F.O. acknowledges the hospitality of MSU and BNL where a portion of this work was performed. This research was supported by the National Science Foundation (grant No. 0100677), RIKEN, Brookhaven National Laboratory, and the U.S. Department of Energy (Contract No. DE-AC02-98CH10886, and No. DE-FG03-95ER40908), and by the Lightner-Sams Foundation.

## References

- [1] CCFR and NuTeV Collab. (M. Goncharov *et al.*), Phys. Rev. **D64**, 112006 (2001); NuTeV Collab. (M. Tzanov *et al.*), hep-ex/0306035.
- [2] NuTeV Collaboration, G.P. Zeller *et al.*, Phys. Rev.Lett. **88**, 091802 (2002); Phys. Rev. **D65**, 111103 (2002), and **D67**, 119902 (2003) (E).
- [3] Phys. Rev. **D65**, 111103 (2002); Erratum ibid **D67**, 119902 (2003).
- [4] V. Barone, C. Pascaud, F. Zomer, Eur. Phys. J. **C12**, 243 (2000); this analysis is currently being updated and early results have been presented by B. Porthault at DIS03; <http://www.desy.de/dis03>.
- [5] J. Pumplin, D. R. Stump, J. Huston, H. L. Lai, P. Nadolsky and W. K. Tung, JHEP **0207**, 012 (2002).
- [6] A.D. Martin, R.G. Roberts, W.J. Stirling, R.S. Thorne, Eur. Phys. J. **C23**, 73 (2002).
- [7] M. Glück, E. Reya and A. Vogt, Eur. Phys. J. **C5**, 461 (1998).
- [8] S. Kretzer, H.L. Lai, F.I. Olness, and W.K. Tung, hep-ph/0307022.
- [9] P. Berge *et al.*, Z. Phys **C49**, 187 (1991).
- [10] J. C. Webb *et al.* [NuSea Collaboration], arXiv:hep-ex/0302019.
- [11] S. Davidson, S. Forte, P. Gambino, N. Rius, A. Strumia, JHEP **0202**, 037, 2002.
- [12] K.S. McFarland and S.-O. Moch, hep-ph/0306052.
- [13] P. Gambino, hep-ph/0211009; A. Strumia, hep-ex/0304039.
- [14] J. Pumplin, D.R. Stump, W.K. Tung, et al., Phys. Rev. **D65**, 014011 (2002); Phys. Rev. **D65**, 014013 (2002); Phys. Rev. **D65**, 014012 (2002).
- [15] S. Kretzer *et al.*, article in preparation.

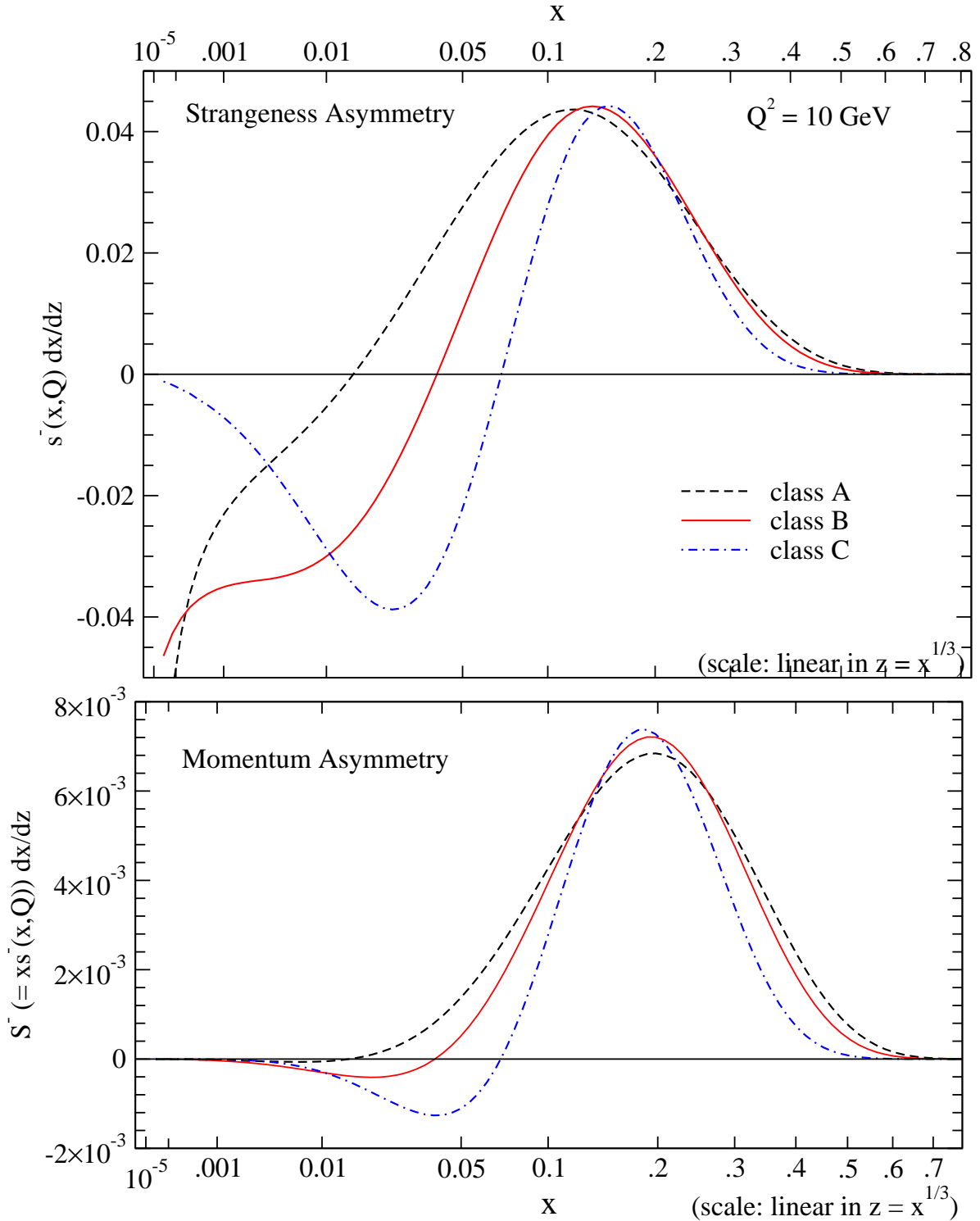


Figure 1: Typical strangeness asymmetry  $s^-(x)$  and the associated momentum asymmetry  $S^-(x)$ . The axes are chosen such that both large and small  $x$  regions are adequately represented, and that the area under each curve equals the corresponding integral.

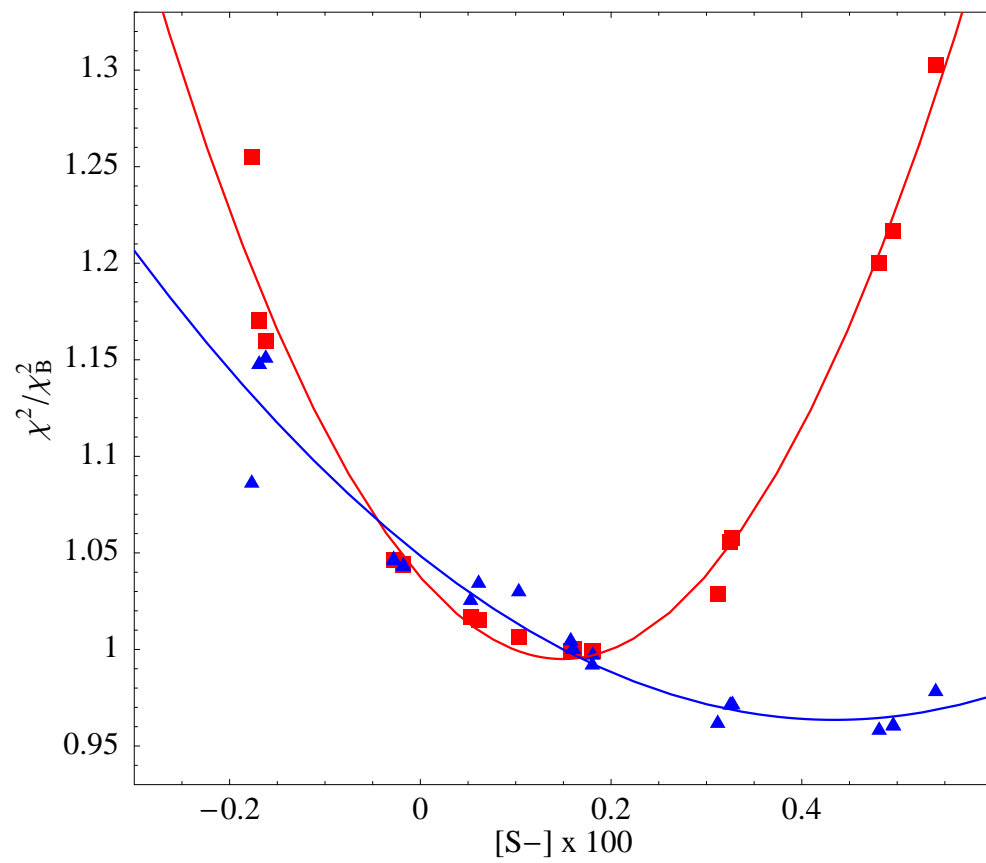


Figure 2: Correlation between  $\chi^2$  values and  $[S^-]$ .

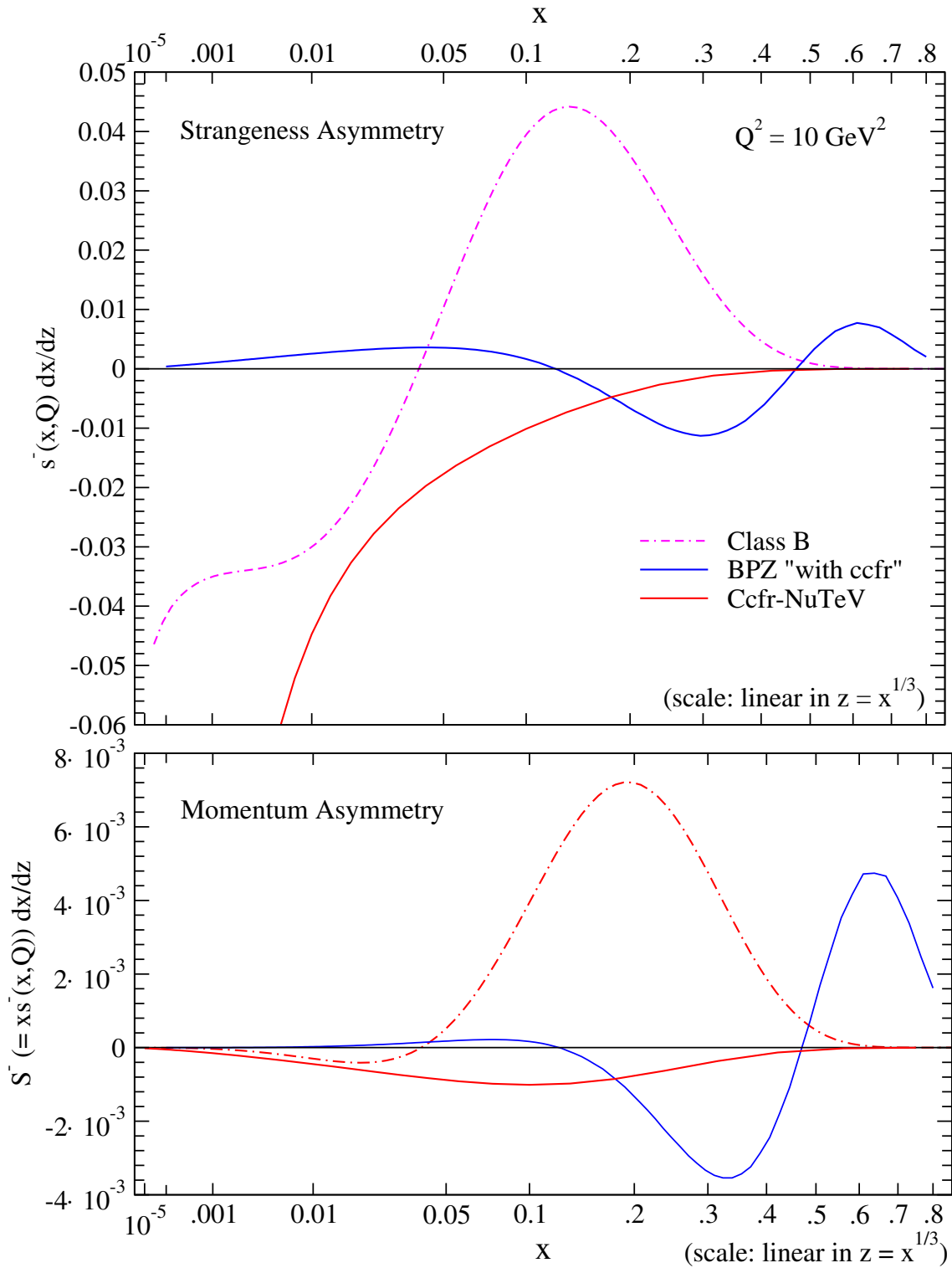


Figure 3: Comparison of  $s^-(x)$  and  $S^-(x)$  functions of our central fit “B” with that of BPZ and CCFR-NuTeV.